*Inorg. Chem.* **2004**, *43*, 3248–3256


# An Electron Localization Function Study of the Geometry of $d^0$ Molecules of the Period 4 Metals Ca to Mn

**Ronald J. Gillespie,*,† Stéphane Noury,† Julien Pilmé,‡ and Bernard Silvi*,‡**

*Department of Chemistry, McMaster University, Hamilton, Ontario L8S 4M1, Canada, and Laboratoire de Chimie Théorique, Université Pierre et Marie Curie, Tour 22, 4 Place Jussieu, 75252 Paris Cédex 05, France*

Received December 5, 2003

We have studied the geometry of the formally $d^0$ $MX_n$ (X = F, H, $CH_3$ and O; $n$ = 2–6) molecules of the period 4 metals from Ca to Mn by studying the topology of the electron localization function (ELF) in order to try to understand why many of these molecules have non-VSEPR geometries. The quantitative analysis of the core basin population shows that it is always larger than its conventional value (18) because, in the LCAO-MO scheme, the 3d basis functions centered on the metal noticeably contribute to the electron density within the core region associated with the M shell. Therefore, the density available to form the bonds is less than $Z(M) - 18$, the value adopted in electron counts. Under the influence of the ligands, these electrons cause the core to lose its spherical symmetry by the formation of opposite-spin pair localization basins, which in turn influence the geometry of the ligands if the interaction of the ligands with the core is sufficiently strong. All of the ligands considered in this study, except F, interact with the core sufficiently strongly to give non-VSEPR geometries, which we have rationalized on the basis of the ELF topology.

## 1. Introduction

It has long been known that many transition-metal molecules do not have the geometry predicted by the VSEPR model or by ligand−ligand repulsion. These deviations from the expected geometry have been explained by the crystal- and ligand-field models as being due to the interaction of the ligands with the d electrons in the core. However, there are many transition-metal molecules, as well as molecules of the period 2 elements, that, formally at least, have no d electrons in the core. These molecules are therefore expected to have spherical $ns^2$ $np^6$ cores and to have geometries in accordance with the VSEPR model or with ligand−ligand repulsion, which both assume a spherical core. However, a large number of such molecules have been found to have "non-VSEPR" geometries. These molecules and the various theories and models that have been used to attempt to explain their geometries have been very thoroughly and extensively reviewed by Kaupp.[1] From this review, it is clear that the geometries of non-VSEPR molecules are by no means fully understood. Most of the previous discussion of the geometry and bonding of these molecules has been based on orbital models. We have taken a different approach based on the analysis of the electron density in an attempt to add fresh insight into the factors determining the geometry of these molecules.

In previous work,[2,3] the electron density of the metal atom core of some fluorides, hydrides, and methanides of Ca, Sr, and Ba and of V and Cr was studied by means of an atoms-in-molecules (AIM) analysis of the electron density and its Laplacian.[4,5] This work showed that the metal atom core is distorted from the spherical shape assumed by the VSEPR model. This nonspherical shape of the core is revealed by the presence of charge concentrations (CCs) in the Laplacian of the density of the M shell. These CCs result from the interaction of the ligands with the core M-shell electrons, that is, from the Pauli repulsion between the ligand electrons and the core M-shell electrons. The geometry of these molecules was rationalized in terms of the frequently competing effects of ligand−ligand repulsion and the

* Author to whom correspondence should be addressed. E-mail: silvi@lct.jussieu.fr.
† McMaster University.
‡ Université Pierre et Marie Curie.

(1) Kaupp, M. *Angew. Chem., Int. Ed. Engl.* **2001**, *40*, 3534.
(2) Bytheway, I.; Gillespies, R. J.; Tang, T.-H.; Bader, R. F. W. *Inorg. Chem.* **1995**, *34*, 2407.
(3) Gillespie, R. J.; Bytheway, I.; Tang, T.-H.; Bader, R. F. W. *Inorg. Chem.* **1996**, *35*, 3954.
(4) Bader, R. F. W. *Atoms in Molecules: A Quantum Theory*; Oxford University Press: Oxford, U.K., 1990.
(5) Popelier, P. L. A. *Atoms In Molecules: an Introduction*; Pearson Education Group: Harlow, U.K., 2000.



10.1021/ic0354015 CCC: $27.50 © 2004 American Chemical Society
Published on Web 04/17/2004

tendency of the ligands to occupy sites that minimize their interaction with the M-shell electrons, namely, the sites of electron depletion that are found in the faces and edges of the polyhedron formed by the CCs. While this work showed that the distortion (polarization) of the core is an important factor in determining the geometry, it did not provide a simple model for the prediction of the geometry. It also left several important questions unanswered such as the following: (1) What determines the number and geometry of the CCs? (2) Why in many molecules do the ligands assume positions that avoid the CCs, thus accounting for their non-VSEPR geometries, while in some molecules the ligands do not avoid the CCs and have VSEPR geometries?

The present paper describes a more extensive study of $d^0$ molecules, using the electron localization function (ELF), in which we have studied the core distortion in the following series of molecules: (1) $CaX_2$, $ScX_3$, $TiX_4$, $VX_5$, and $CrX_6$ where X = H, F, $CH_3$; (2) $ScO_2^-$, $TiO_2$, $VO_2^+$, and $CrO_2^{2+}$; (3) $VO_3^-$, $CrO_3$, and $MnO_3^+$.

## 2. ELF and Its Topological Analysis

The Lewis concept of bonding and nonbonding electron pairs is a fundamental and extremely useful concept in chemistry. The formation of electron pairs in the valence shell of an atom in a molecule is a consequence of the Pauli principle, according to which the total wave function for a molecule must be antisymmetric to electron interchange. As a consequence the probability of finding two electrons with identical spins very close together is less than that for two electrons with antiparallel spins. In other words, there is an effective Pauli repulsion between parallel spin electrons but no Pauli repulsion between antiparallel spin electrons. In a molecule of a nonmetal from groups 13−18, the attraction of the ligands for the electrons of the central atom in conjunction with the Pauli repulsion between like spin electrons creates regions in the electron density of the valence shell where there is a high probability of finding a pair of electrons of opposite spin, that is, where the number of pairs of electrons of opposite spin is greater than the number of pairs with the same spin. These regions correspond to the bonding and lone pairs of the Lewis model.[6,7] The number of electrons with the same spin that a given electron has around it within an elementary volume can be taken as a good measure of the Pauli repulsion between same-spin electrons. Becke and Edgecombe's ELF[8−11] is derived from this measure of Pauli repulsion and is confined to the [1, 0] interval. It tends to 1 where parallel spins are highly improbable and where there therefore is a high probability of opposite-spin pairs and to zero in regions where there is a high probability of same-spin pairs.

Another local descriptor of the pair formation in the sense of Lewis's model, the so-called spin pair composition, has recently been introduced on the basis of the two-particle probability density analysis.[11] This function is defined as the ratio of same-spin and opposite-spin pair functions integrated over a sampling volume around the reference point (see appendix A). It has been shown that ELF is an excellent approximation to this function. ELF has the advantage that it can be expressed analytically in terms of basis functions in all practical cases where the wave function is expressed in terms of orbitals, whereas the spin pair composition must be calculated numerically.

The regions of high and low opposite electron spin probability can be defined by the topological analysis of ELF.[12,13] By means of its gradient vector field, this topological analysis partitions the molecular space into basins, each of which surrounds an attractor at which ELF has a local maximum value. For the molecules of the elements from groups 13−18, these localization basins are consistent with the Lewis description of an atom in a molecule consisting of a central core and a valence shell consisting of bond pairs and lone pairs. The basins of ELF are classified as core basins labeled C(A), where A is the symbol of the central atom, and as valence basins. The valence basins are characterized by the number of core basins with which they share a boundary. This number is called the synaptic order. Thus, there are monosynaptic, disynaptic, trisynaptic basins, and so on. Monosynaptic basins, labeled V(A), correspond to the lone pairs of the Lewis model and polysynaptic basins to the shared pairs of the Lewis model. In particular, disynaptic basins, labeled V(A,X), correspond to two-center bonds, trisynaptic basins, labeled V(A,X,Y), to three-center bonds, and so on. The basins in a given valence shell have the same geometry as the qualitative domains of the VSEPR model. In a free atom, there is one core basin for each core shell whose attractors are degenerated on concentric spheres corresponding to the core shells, except for the K shell, for which the basin is a sphere centered on the nucleus. In molecules of the nonmetals, the spherical symmetry of the outer or valence shell is broken and it is split into monosynaptic and polysynaptic, usually disynaptic, basins. In molecules of the elements of period 4 from groups 1−12, the M shell undergoes a significant distortion because of the interaction with the surrounding valence basins and splits into several basins. These M-shell basins and their effect on the geometry of a molecule are the particular object of the present study.

By integration of the one-electron density over any of the core or valence basin volumes, their population, $\bar{N}(\Omega_i)$ and the variance $\sigma^2[\bar{N}(\Omega_i)]$ of the population, which is a measure of the quantum mechanical uncertainty of the basin as a consequence of electron delocalization, may be determined (see Appendix B).

A similar topological analysis of the electron density of a molecule partitions it into its component atomic basins. This

(6) Gillespie, R. J.; Robinson, E. A. *Angew. Chem., Int. Ed. Engl.* **1996**, *35*, 495.
(7) Gillespie, R. J.; Popelier, P. L. A. *Chemical Bonding and Molecular Geometry*; Oxford University Press: Oxford, U.K., 2001.
(8) Becke, A. D.; Edgecombe, K. E. *J. Chem. Phys.* **1990**, *92*, 5397.
(9) Dobson, J. F. *J. Chem. Phys.* **1991**, *94*, 4328.
(10) Savin, A.; Jepsen, O.; Flad, J.; Andersen, O. K.; Preuss, H.; von Schnering, H. G. *Angew. Chem., Int. Ed. Engl.* **1992**, *31*, 187.
(11) Silvi, B. *J. Phys. Chem. A* **2003**, *107*, 3081.
(12) Silvi, B.; Savin, A. *Nature* **1994**, *371*, 683.
(13) Häussermann, U.; Wengert, S.; Nesper, R. *Angew. Chem., Int. Ed. Engl.* **1994**, *33*, 2069.

partitioning is the basis of the AIM theory.[4,5] This theory makes use of the Laplacian of the electron density to determine where the electron density is locally concentrated and where it is locally depleted. The Laplacian exhibits the shell structure of the atom, and the number and geometry of the maxima in the valence shell also correspond to the electron pairs of the Lewis model and their geometry as described by the VSEPR model. This was the method of analysis of the electron density that we used in an earlier work.[2,3]

## 3. Computational Methods

The ab initio calculations have been performed at the hybrid Hartree−Fock density functional B3LYP level[14−17] with Gaussian 98 software.[18] The geometries have been optimized with the 6-311G(2d,2p) basis set.[19−23] The analysis of the ELF function has been carried out with the TopMoD program developed in the Laboratoire de Chimie Théorique de l'Université Pierre et Marie Curie,[24,25] and the ELF isosurface has been visualized with Amira 3.0 software.[26]

## 4. Results and Discussion

Table 1 gives the calculated bond angles and bond lengths for the $MX_n$ molecules of Ca, Sc, Ti, V, and Cr (X = F, H, Me). This table also gives the populations of the ligand, the disynaptic basins, the core together with its variance, and the excess core population. Previous calculations of the molecules $VH_5$ and $CrH_6$ have given several different structures of similar energy that were basis set and calculation method dependent, were not in agreement with each other, and were different from the calculated structures of $VF_5$ and $V(CH_3)_5$ and of $CrF_6$ and $Cr(CH_3)_6$.[27−31] In the present work, we have found $C_{4v}$ and $C_3$ structures for $VH_5$ and $CrH_6$, respectively. The structure of $CrH_6$ is very distorted and appears to be influenced by weak hydrogen−hydrogen bonding. Table 2 gives analogous data for the $MO_2$ and $MO_3$ molecules and ions of Sc, Ti, V, Cr, and Mn.

**Table 1.** Bond Angles (deg), Internuclear Distances (pm), Ligand Atomic Populations, Disynaptic Valence Basin Populations, Metal Core Basin Population, Valence Density Deficit Δ, and Variance[a]

| molecule | group | ∠XMX | *R*(MX) | *N*(X) | *V*(M,X) | *C*(M) | Δ | $\sigma^2$ |
|---|---|---|---|---|---|---|---|---|
| KF | $C_{\infty v}$ | | 215.5 | 9.84 | | 18.08 | 0.08 | 0.21 |
| $CaF_2$ | $C_{2v}$ | 140.4 | 198.0 | 9.80 | | 18.25 | 0.25 | 0.48 |
| $ScF_3$ | $D_{3h}$ | 120.0 | 183.8 | 9.71 | | 18.65 | 0.65 | 0.95 |
| $TiF_4$ | $T_d$ | 109.4 | 174.6 | 9.47 | | 19.20 | 1.20 | 1.51 |
| $VF_5$ | $D_{3h}$ | 180.0 | 174.3 | 9.51 | | 19.93 | 1.93 | 1.95 |
| $CrF_6$ | $O_h$ | 120.0 | 170.8 | 9.49 | | | | |
| KH | $C_{\infty v}$ | 90.0 | 172.4 | 7.44 | | 20.81 | 2.81 | 2.47 |
| $CaH_2$ | $C_{2v}$ | | 224.2 | 1.72 | 1.88 | 18.09 | 0.09 | 0.22 |
| $ScH_3$ | $C_{3v}$ | 139.8 | 202.1 | 1.74 | 1.93 | 18.13 | 0.13 | 0.39 |
| $TiH_4$ | $T_d$ | 117.7 | 180.3 | 1.60 | 1.84 | 18.61 | 0.61 | 0.88 |
| $VH_5$ | $C_{4v}$ | 109.4 | 168.8 | 1.38 | 1.70 | 19.40 | 1.40 | 1.44 |
| $CrH_6$ | $C_{3v}$ | 121.6 | 164.9 | 1.43 | 1.70 | 20.21 | 2.21 | 1.88 |
| $KCH_3$ | $C_{3v}$ | 90.0 | 159.8 | 1.27 | 1.52 | | | |
| $Ca(CH_3)_2$ | $C_{2v}$ | 119.6 | 157.5 | 1.28 | 1.56 | 21.40 | 3.40 | |
| $Sc(CH_3)_3$ | $C_{3v}$ | 60.0 | 151.7 | 1.08 | 1.30 | | | |
| $Ti(CH_3)_4$ | $T_d$ | | 260.5 | 6.64 | 1.86 | 18.13 | 0.13 | 0.24 |
| $V(CH_3)_5$ | $C_{2v}$ | 128.6 | 240.6 | 6.67 | 2.03 | 18.20 | 0.20 | 0.45 |
| | | 116.6 | 219.5 | 6.69 | 1.91 | 18.64 | 0.64 | 0.87 |
| $Cr(CH_3)_6$ | $C_3$ | 109.4 | 208.3 | 6.62 | 1.71 | 19.30 | 1.30 | 1.46 |
| | | 112.1 | 201.6 | 6.58 | 1.67 | 20.16 | 2.16 | 1.95 |
| | | 81.7 | 207.7 | 6.46 | 1.47 | | | |
| | | 90.6 | 203.1 | 6.43 | 1.43 | 21.11 | 3.11 | 2.33 |
| | | 77.4 | 210.6 | 6.34 | 1.26 | | | |

[a] For $VF_5$, first line axial ligand and second line equatorial ligands. For $VH_5$ and $V(CH_3)_5$, first line axial ligand and second line ligands in $\sigma_v$ planes. For $CrH_6$ and $Cr(CH_3)_6$, first and second lines correspond to the two groups of symmetry-related ligands.

**Table 2.** Bond Angles (deg), Internuclear Distances (pm), Ligand Atomic Populations, Metal−Ligand Delocalization Indexes, Metal Core Basin Population, Valence Density Deficit Δ, and Variance

| molecule | group | ∠XMX | *R*(MX) | *N*(X) | *C*(M) | Δ | $\sigma^2$ |
|---|---|---|---|---|---|---|---|
| $ScO_2^-$ | $C_{2v}$ | 121.9 | 177.7 | 9.31 | 18.96 | 0.96 | 1.23 |
| $TiO_2$ | $C_{2v}$ | 111.0 | 163.0 | 8.93 | 19.66 | 1.66 | 1.68 |
| $VO_2^+$ | $C_{2v}$ | 106.2 | 154.6 | 8.51 | 20.39 | 2.39 | 2.13 |
| $CrO_2^{2+}$ | $C_{2v}$ | 104.3 | 150.7 | 8.08 | 21.22 | 3.22 | 2.40 |
| $VO_3^-$ | $C_{3v}$ | 117.2 | 164.2 | 9.02 | 20.22 | 2.22 | 2.16 |
| $CrO_3$ | $C_{3v}$ | 113.4 | 157.3 | 8.67 | 21.08 | 3.08 | 2.51 |
| $MnO_3^+$ | $C_{3v}$ | 110.6 | 154.2 | 8.32 | 22.08 | 4.08 | 2.75 |

**4.1. Population of the Metal Atom Core Basin.** The ability of the ELF function to display the shell structure of atoms has been qualitatively shown in the paper of Becke and Edgecombe[8] and studied qualitatively by Kohout and Savin.[32] In a recent paper, Kohout et al.[33] have given an enlightening discussion of this property that we will summarize here in order to clarify some important points. The ELF partition provides a position space representation of the atom in terms of concentric nonoverlapping regions or shells, and there is no further subshell structuring. In the orbital-


(14) Becke, A. D. *J. Chem. Phys.* **1993**, *98*, 5648.
(15) Becke, A. D. *Phys. Rev.* **1988**, *A38*, 3098.
(16) Lee, C.; Yang, Y.; Parr, R. G. *Phys. Rev.* **1988**, *B37*, 785.
(17) Miechlich, B.; Savin, A.; Stoll, H.; Preuss, H. *Chem. Phys. Lett.* **1989**, *157*, 200.
(18) Frisch, M. J.; Trucks, G. W.; Schlegel, H. B.; Scuseria, G. E.; Robb, M. A.; Cheeseman, J. R.; Zakrzewski, V. G.; Montgomery, A., Jr.; Stratmann, R. E.; Burant, J. C.; Dapprich, S.; Millam, J. M.; Daniels, A. D.; Kudin, K. N.; Strain, M. C.; Farkas, O.; Tomasi, J.; Barone, V.; Cossi, M.; Cammi, R.; Mennucci, B.; Pomelli, C.; Adamo, C.; Clifford, S.; Ochterski, J.; Petersson, G. A.; Ayala, P. Y.; Cui, Q.; Morokuma, K.; Malick, D. K.; Rabuck, A. D.; Raghavachari, K.; Foresman, J. B.; Cioslowski, J.; Ortiz, J. V.; Baboul, A. G.; Stefanov, B. B.; Liu, G.; Liashenko, A.; Piskorz, P.; Komaromi, I.; Gomperts, R.; Martin, R. L.; Fox, D. J.; Keith, T.; Al-Laham, M. A.; Peng, C. Y.; Nanayakkara, A.; Challacombe, M.; Gill, P. M. W.; Johnson, B.; Chen, W.; Wong, M. W.; Andres, J. L.; Gonzalez, C.; Head-Gordon, M.; Replogle, E. S.; Pople, J. A. *Gaussian 98*, Revision A.9; Gaussian Inc.: Pittsburgh, PA, 1998.
(19) Wachters, A. J. H. *J. Chem. Phys.* **1970**, *52*, 1033.
(20) Clark, T.; Chandrasekhar, J.; Spitznagel, G. W.; von Ragué Schleyer, P. *J. Comput. Chem.* **1983**, *4*, 294.
(21) Frisch, M. J.; Pople, J. A.; Binkley, J. S. *J. Chem. Phys.* **1984**, *80*, 3265.
(22) MacLean, A. D.; Chandler, G. S. *J. Chem. Phys.* **1980**, *72*, 5639.
(23) Krishnan, R.; Binkley, J. S.; Seeger, R.; Pople, J. A. *J. Chem. Phys.* **1980**, *72*, 650.
(24) Noury, S.; Krokidis, X.; Fuster, F.; Silvi, B. Topmod package, 1997.
(25) Noury, S.; Krokidis, X.; Fuster, F.; Silvi, B. *Comput. Chem.* **1999**, *23*, 597.
(26) Amira 3.0 TGS, Template Graphics Sofware, Inc., San Diego, CA, 2002.
(27) Kang, S. K.; Tang, H.; Albright, T. A. *J. Am. Chem. Soc.* **1993**, *115*, 1971.
(28) Clark, R.; Landis, T.; Cleveland, T. K. F. *J. Am. Chem. Soc.* **1995**, *117*, 1859.
(29) Tanpipat, N.; Baker, J. *J. Phys. Chem.* **1996**, *100*, 19818.
(30) Ma, B.; Collins, C. L.; Schaefer, H. F., III. *J. Am. Chem. Soc.* **1996**, *118*, 870.
(31) Bayse, C. A.; Hall, M. B. *J. Am. Chem. Soc.* **1999**, *121*, 1348.
(32) Kohout, M.; Savin, A. *Int. J. Quantum Chem.* **1996**, *60*, 875.
(33) Kohout, M.; Wagner, F. R.; Grin, Y. *Theor. Chem. Acc.* **2002**, *108*, 150.

based representation, a shell is defined as the set of occupied atomic orbitals with a given principal quantum number. The two representations provide the same number of shells, and the "ELF shell" populations are always close to the occupation numbers of the corresponding "orbital shell". However, in Hartree−Fock calculations, all of the orbitals contribute to each "ELF shell" population. The ELF analysis of the free atoms of the period 4 elements, displays three core shells (K, L, and M) and a valence shell (N). In these atoms, the population of the valence shell (N) is close to either 1 or 2 for groups 1−12 or lies in the range of 3−8 for the main group 13−18 elements.[32] In the orbital representation, the electrons assigned to the 3s and 3p subshells are considered as core electrons for all of the period 4 elements, whereas those of the 3d subshell are valence electrons for the group 1−12 elements but core electrons for the group 13−18 elements. Accordingly, for the elements of groups 1−12, the core population is considered to be 18, while $Z - 18$ electrons are considered to be involved in the formation of bonds (ionic or covalent) and therefore to be valence electrons. This latter a priori partition is not relevant in the topological representation because the valence density is defined by different criteria, i.e., its spacial location within the outermost basins. In the series of fluorides investigated here, the metal M-shell population $\bar{N}$[C(M)] ranges from 18.25 for Ca to 20.81 for Cr so that the contribution of the metal atom to the integrated valence density is less than the $Z - 18$ "valence" 3d and 4s electrons considered to be used in the bond formation by the conventional electron count. According to the ELF topological analysis, the core has a population of $18 + \Delta$ electrons, where $\Delta$ can be interpreted as the valence density deficit, or the core excess density, with respect to the standard electron count. It may be seen in Table 1 that in each of the series of fluorides, hydrides and methanides $\Delta$ increases from Ca to Cr. From these values it may be seen that for the Ca molecules, as expected, very nearly two Ca electrons are used in bond formation. However, from Sc to Cr, the values of $\Delta$ show that the metal participation to the valence shell, and therefore to the bonding, exceeds two electrons with difficulty. For example, for the fluorides this contribution amounts to 2.35 for Sc and to 3.19 for Cr, instead of 3 and 6 as expected from the electron count. Table 2 shows that for the dioxides the $\Delta$ increases from Sc to Cr and for the trioxides from V to Mn and is larger than that for the fluorides, hydrides, and methanides. The reason for the difficulty of using more than two electrons for bond formation may be considered to be the very high effective electronegativity of the $M^{2+}$ cations, which are 18.77 eV for $Sc^{2+}$ and 24.96 eV for $Cr^{2+}$ compared to 10.23 eV for fluorine on the Mulliken scale (the average of the second and third ionization energies).

To link the ELF basin population analysis with the simple representation based on electron count, we formally interpret the core population in terms of a superposition of oxidation states, or of core states, of the form [Ar] $d^n$. The weight of each configuration is determined from the values of $\bar{N}$[C(M)] and of their variance by solving the linear system

$$\bar{N}[\mathrm{C(M)}] = \sum_{n=0}^{3} w_n(18 + n)$$

$$\sigma^2 = \sum_{n=0}^{3} w_n(18 + n - \bar{N}[\mathrm{C(M)}])^2$$

$$\sum_{n=0}^{3} w_n = 1 \qquad (1)$$

For closed-shell systems, $n$ is restricted to even values, namely, 0, 2, and 4, which yields the weights in Table 3.

**4.2. Molecular Geometry.** The geometry of nonmetal molecules with no lone pairs of electrons in the valence shell is determined by bond−bond repulsion according to the VSEPR model or by ligand−ligand repulsion. The predictions of these two models are exactly the same and for homoleptic molecules give the well-known $AX_2$ linear, $AX_3$ planar-triangular, $AX_4$ tetrahedral, $AX_5$ trigonal-bipyramidal, and $AX_6$ octahedral geometries. Both models are based on the assumption that the core has a spherical shape, as is the case for molecules of the elements of period 2, which have a $1s^2$ core, and those of period 3, with a [Ne] core. However, as we have seen, the molecules of the period 4 elements, which are formally expected to have an [Ar] core, have a core population of more than 18 electrons. It is the deviation of the actual core population with respect to the conventional expectation that is responsible for the non-VSEPR geometries of the molecules of the elements of groups 2−12 in period 4. The interaction of the ligands with the external core shell electron density causes the partial localization of the electrons into opposite-spin pairs and therefore the formation of localization basins in ELF, which in turn can influence the geometry of the ligands. Such a structuring of the ELF core basins has been previously reported for lanthanide halides[34] and later discussed by Kohout et al. in a more general context.[33] We have found that the number and geometry of the M-shell localization basins in ELF are the same as the number and geometry of the M-shell CCs in the Laplacian of the density in those molecules where both functions have been studied.[2,3]

Table 4 gives the number, type, and geometry of the core basins, together with the value of ELF at the attractor, the volume, and the population of each core basin. In every case, there are at least four core localization basins, and in every case, there are core basins on the opposite side of the core from each ligand, called ligand-opposed (LO) core basins, and additional core basins that are not LO, called NLO core basins. The information provided by the ELF analysis supports a simplified model in terms of interacting electron pairs, which generalizes the VSEPR ideas to both valence and external core shell electrons. On the one hand, the Pauli repulsion between the ligand electrons and the core electrons localizes a pair of opposite-spin electrons at as great a distance as possible from the ligand, that is, in the LO positions, which corresponds in the ELF picture to the LO

(34) Joubert, L.; Silvi, B.; Picard, G. *Theor. Chem. Acc.* **2000**, *1046*, 109.

**Table 3.** Weights of the [Ar] $d^n$ Resonant Core Configurations Which Model the Core Populations and Their Variances

| molecule | [Ar] | [Ar] $d^2$ | [Ar] $d^4$ |
|---|---|---|---|
| $CaF_2$ | 0.880 | 0.115 | 0.005 |
| $ScF_3$ | 0.684 | 0.307 | 0.009 |
| $TiF_4$ | 0.469 | 0.462 | 0.069 |
| $VF_5$ | 0.262 | 0.511 | 0.227 |
| $CrF_6$ | 0.188 | 0.218 | 0.594 |
| $CaH_2$ | 0.953 | 0.028 | 0.019 |
| $ScH_3$ | 0.699 | 0.297 | 0.004 |
| $TiH_4$ | 0.375 | 0.550 | 0.075 |
| $VH_5$ | 0.188 | 0.519 | 0.293 |
| $CrH_6$ | 0.150 | 0.0 | 0.850 |
| $Ca(CH_3)_2$ | 0.911 | 0.078 | 0.011 |
| $Sc(CH_3)_3$ | 0.680 | 0.320 | 0.0 |
| $Ti(CH_3)_4$ | 0.426 | 0.498 | 0.076 |
| $V(CH_3)_5$ | 0.207 | 0.506 | 0.287 |
| $Cr(CH_3)_6$ | 0.168 | 0.109 | 0.723 |
| $ScO_2^-$ | 0.520 | 0.480 | 0.0 |
| $TiO_2$ | 0.309 | 0.551 | 0.140 |
| $VO_2^+$ | 0.188 | 0.429 | 0.383 |
| $CrO_2^{2+}$ | 0.181 | 0.028 | 0.791 |
| $VO_3^-$ | 0.221 | 0.448 | 0.331 |
| $CrO_3$ | 0.190 | 0.081 | 0.729 |

**Table 4.** M-Shell Basins: Number, Type (LO, Ligand Opposed; NLO, Not Opposed; LD, Ligand Directed; CIRC, Toroidal; ax, Axial; eq, Equatorial), ELF Value at the Attractor, Volume ($bohr^3$), and Population, and Geometry (tri, Triangular; pyr, Pyramidal; trig, Trigonal; octah, Octahedral; tetrah, Tetrahedral; dist, Distorted; sq, Square Pyramidal)

| molecule | group | *n* | type | $\eta$ | geometry | *V* | *N* |
|---|---|---|---|---|---|---|---|
| KF | $C_{\infty v}$ | 2 | CIRC | 0.885 | | 103.5 | 6.08 |
| | | LO | 0.889 | | | 38.7 | 1.95 |
| $CaF_2$ | $C_{2v}$ | 4 | 2 LO | 0.889 | tri pyr | 19.82 | 2.04 |
| | | 2 NLO | 0.892 | | | 18.62 | 2.08 |
| $ScF_3$ | $D_{3h}$ | 5 | 3 LO | 0.893 | trig prism | 9.43 | 1.99 |
| | | 2 NLO | 0.882 | | | 9.40 | 1.33 |
| $TiF_4$ | $T_d$ | 4 | 4 LO | 0.900 | tetrah | 2.40 | 2.28 |
| $VF_5$ | $D_{3h}$ | 5 | 3 LO | 0.873 | trig prism | 6.81 | 2.28 |
| | | 2 NLO | 0.857 | | | 3.50 | 1.46 |
| $CrF_6$ | $O_h$ | 6 | 6 LD | 0.839 | octah | 3.82 | 1.77 |
| KH | $C_{\infty v}$ | 2 | CIRC | 0.887 | | 107.86 | 6.50 |
| | | LO | 0.882 | | | 36.72 | 1.57 |
| $CaH_2$ | $C_{2v}$ | 4 | 2 LO | 0.894 | tri pyr | 17.19 | 1.73 |
| | | 2 NLO | 0.897 | | | 20.24 | 2.33 |
| $ScH_3$ | $C_{3v}$ | 5 | 3 LO | 0.917 | trig prism | 10.83 | 2.0 |
| | | 1 NLO | 0.913 | | | 11.13 | 2.11 |
| | | 1 NLO | 0.880 | | | 3.87 | 0.44 |
| $TiH_4$ | $T_d$ | 4 | 4 LO | 0.936 | tetrah | 2.86 | 2.29 |
| $VH_5$ | $C_{4v}$ | 5 | 1 LO | 0.862 | sq pyr | 3.87 | 1.61 |
| | | 4 LO | 0.917 | | | 6.44 | 2.11 |
| $CrH_6$ | $C_{3v}$ | 6 | 3 LO | 0.891 | dist octah | 5.06 | 1.81 |
| | | 3 LD | 0.921 | | | 4.26 | 1.92 |
| $KCH_3$ | $C_{3v}$ | 4 | 1 LO | 0.881 | tri pyr | 41.13 | 0.70 |
| | | 3 NLO | 0.887 | | | 66.77 | 7.30 |
| $Ca(CH_3)_2$ | $C_{2v}$ | 4 | 2 LO | 0.898 | tri pyr | 19.24 | 1.79 |
| | | 2 NLO | 0.897 | | | 19.92 | 2.31 |
| $Sc(CH_3)_3$ | $C_{3v}$ | 5 | 3 LO | 0.917 | trig prism | 19.24 | 2.02 |
| | | 1 NLO | 0.917 | | | 19.92 | 2.32 |
| | | 1 NLO | 0.907 | | | 2.0 | 0.20 |
| $Ti(CH_3)_4$ | $T_d$ | 4 | 4 LO | 0.955 | tetrah | 8.93 | 2.29 |
| $V(CH_3)_5$ | $C_{2v}$ | 5 | 1 LO | 0.833 | sq pyr | 5.34 | 1.94 |
| | | 4 LO | 0.909 | | | 5.87 | 2.02 |
| $Cr(CH_3)_6$ | $C_3$ | 6 | 3 LO | 0.880 | trig prism | 4.22 | 1.86 |
| | | 3 LO | 0.873 | | | 4.02 | 1.78 |

core basins. On the other hand, the Pauli repulsion between two opposite-spin electron pairs of the M shell in the LO position and the remaining electrons of this latter shell necessarily leads to the formation of at least two other pairs, which is consistent with the number of localization basins belonging to the external core shell. The formation of these

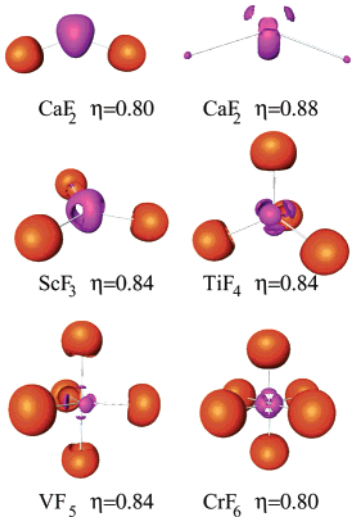


**Figure 1.** ELF localization domains of $MF_n$ molecules. Color code: magenta, cores; red brick, V(F).

core localization basins is analogous to the formation of a total of four bonding and nonbonding (lone-pair) localization basins in the octet valence shell of the main group central atom with at least two ligands.

As we will show, the geometry of the molecules of the metals of period 4 can be rationalized by assuming that they are determined by (1) ligand−ligand repulsion and/or by bond−bond repulsion and (2) the interaction of the ligands with the core M shell, which produces the core localization basins, which in turn may influence the geometry of the ligands.

In general, the M-shell core attractors form a polyhedron that is closely related to the polyhedron formed by the ligands. The positions of minimum spin pair localization are in the middle of the faces of the polyhedron of attractors, and there are also positions of reduced spin pair localization in the middle of each edge of the polyhedron. As we will see, strongly interacting ligands prefer to occupy sites facing these positions of reduced or minimum spin pairing, in which the distances between the ligands and the core attractors are maximized.

In the following discussion, we deal in turn with the $MF_n$, $M(CH_3)_n$, $MH_n$, and $MO_n$ molecules.

**$MF_n$.** $ScF_3$, $TiF_4$, $VF_5$, and $CrF_6$ all have the VSEPR or ligand−ligand repulsion geometries, while $CaF_2$ has a bent rather than the predicted linear geometry. $CaF_2$ has four M-shell localization basins with a disphenoidal $C_{2v}$ geometry, two of which are LO and the other two of which form an arc-shaped basin in which there are two maxima and which is resolved into two basins at higher $\eta$ values. These two NLO basins arise from the interaction of the two LO basins with the other electrons of the core. The two ligands are situated opposite to two of the faces of the disphenoid (Table 4 and Figure 1), thus maximizing their distances from the core attractors.

We expect the degree of distortion of the $CaF_2$ molecule from the linear VSEPR geometry to be relatively small because the excess number of core electrons is very small. The bending of the molecule is opposed by ligand−ligand

interactions. However, ligand−ligand repulsions are also expected to be rather weak because of the large distance between the ligands so that the large bond angle of 140.4° is a result of a compromise between weak ligand−ligand repulsion and weak core-basin−ligand repulsion. Consequently, we also expect this molecule to be rather flexible and the bending vibrational mode to have a large amplitude, as has been observed. That the formation of four partially localized pairs of electrons in the M shell of the metal atom is the explanation for the angular shape of $CaX_2$ molecules was first suggested as long ago as 1972,[35,36] but no evidence in favor of this explanation was available at the time.

If the wave function for the $CaF_2$ molecule is calculated without any contribution from d orbitals, a linear geometry is obtained, confirming that the presence of d electrons in the M shell is a requirement for the molecule to be angular rather than linear. If d electrons are included, then the linear energy geometry has a higher energy than the bent geometry and the M-shell localization basins consist of a torus surrounding the Ca nucleus and two LO localization basins. In the linear molecule, the two ligands are necessarily opposite to these two localization basins, consistent with the higher energy of the linear molecule.

**$ScF_3$.** $ScF_3$ has a planar $D_{3h}$ geometry, suggesting that ligand−ligand repulsions determine the geometry. There are five core basins in the form of a $D_{3h}$ trigonal bipyramid. Three are LO, and the other two complete the trigonal bipyramid. (In Figure 1, the five basins are not fully resolved.) The two additional NLO basins result from the remaining core electrons. Each of these NLO basins has a population of approximately one electron. Each of the three ligands faces one of the three edges of the trigonal bipyramid of localization basins, so that they are in positions of reduced interaction with the core but not in positions of minimum interaction, which would be in three of the faces of the trigonal bipyramid of localization basins. Ligand−ligand repulsion prevents the ligand from adopting the positions of minimum interaction with the core.

**$TiF_4$.** $TiF_4$ has a tetrahedral geometry with four LO core basins that form a tetrahedron reciprocal to the tetrahedron of ligands (Figure 1). Thus, each ligand is situated opposite to a face of this tetrahedron of core basins in a region of maximum decreased localization of opposite spins so that they have a minimum interaction with the core. The tetrahedral geometry of $TiF_4$ is therefore determined by ligand−ligand repulsions reinforced by ligand−core repulsions.

**$VF_5$.** $VF_5$ has a trigonal-bipyramidal $D_{3h}$ geometry with a similar trigonal-bipyramidal geometry of core basins, each of which is LO (Figure 1), so that the trigonal bipyramid of core basins is rotated through 60° with respect to the trigonal bipyramid of ligands. Thus, the three equatorial ligands face the three equatorial edges of the trigonal bipyramid of core basins and so are in positions of reduced, but not minimum, interaction with the core basins. The axial ligands directly face a core basin and so are in positions of maximum interaction with the core basins. Clearly, ligand−ligand interactions determine the geometry of this molecule.

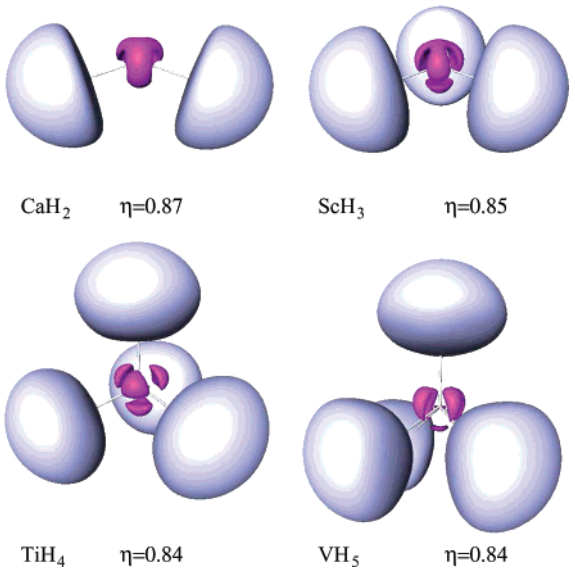


**Figure 2.** ELF localization domains of $MH_n$ molecules, M = Ca−V. Color code: magenta, cores; light blue, V(M,H).

**$CrF_6$.** $CrF_6$ has an octahedral $O_h$ geometry with a similar octahedron of LO core basins so that each ligand faces a core basin (Figure 1) and therefore ligand−ligand interactions determine the geometry. As in all of the other fluorides, it appears that the interaction of a fluorine ligand with the core is very weak.

**Hydrides and Methanides.** The hydrides and methanides, with the exception of $CaH_2$ and $Ca(CH_3)_2$, have geometries different from those of the fluorides because methyl and hydrogen ligands interact more strongly with the core than fluorine ligands and therefore have a stronger preference for sites of weak opposite-spin pair localization than fluorine ligands. The geometries and localization domains for all of the hydrides except $CrH_6$ are shown in Figure 2.

**$CaH_2$ and $Ca(CH_3)_2$.** Both of these molecules have non-VSEPR bent geometries such as $CaF_2$. In all of these molecules, there are two LO core basins and two further basins completing a disphenoid of core basins. The ligands are situated opposite to two of the faces of the disphenoid of core basins in positions of minimum ligand−core interaction. Thus, core interactions dominate the geometry of these molecules as well as that of $CaF_2$.

**$ScH_3$ and $Sc(CH_3)_3$.** Unlike $ScF_3$, these two molecules have a $C_{3v}$ pyramidal geometry. There are five core basins with a trigonal-bipyramidal geometry, although the two axial basins are not equivalent. Because of their stronger interaction with the core than a fluorine ligand, the ligands have moved away from the edges of the trigonal bipyramid of core basins, the positions occupied by the fluorine ligands in $ScF_3$, into the faces of the trigonal bipyramid of core basins, thus reducing their interaction with the core basins. $Sc(CH_3)_3$ has three Sc−C disynaptic basins, each of which is expected to interact strongly with a core basin so that there is a strong tendency for a $CH_3$ ligand to seek a site that

(35) Gillespie, R. J. *Molecular Geometry*; Van Nostrand Reinhold: London, 1972.
(36) Gillespie, R. J.; Hargittai, I. *The VSEPR Model of Molecular Geometry*; Allyn and Bacon: Boston, MA, 1991.

minimizes its interaction with the core, that is, a position opposite to one of the faces of the core basin polyhedron. A hydride ligand has a single combined core and disynaptic basin, called a protonated disynaptic basin, and behaves just like a $CH_3$ ligand.

**$TiH_4$ and $Ti(CH_3)_4$.** Both of these molecules have a tetrahedral $T_d$ geometry, with four LO core basins forming a tetrahedron reciprocal to the tetrahedron of ligands. So, the ligands are in positions of minimum interaction with the core basins, and there is no reason for the molecule to distort from the tetrahedral geometry determined by ligand−ligand repulsion. It seems reasonable to predict that all $TiX_4$ molecules, where X is a monatomic ligand, will have a tetrahedral geometry.

**$VH_5$ and $V(CH_3)_5$.** Unlike the trigonal-bipyramidal $VF_5$ molecule, both of these molecules have a square-pyramidal $C_{4v}$ geometry in which there is a reciprocal square pyramid of LO core basins. The axial ligand is in front of the square face of the square pyramid of core basins, and the other four ligands are in front of the four edges of the triangular faces. All of the ligands are thus in positions of minimum interaction with the core. In these molecules, the geometry is determined by the minimization of ligand−core interactions. The trigonal bipyramid of core localization basins found for $VF_5$ has six triangular faces. However, the five ligands can only occupy positions opposite to five of these faces, giving a very unsymmetrical structure with small bond angles. It is well-known from studies of $AX_5$ nonmetal molecules that the square pyramid has only a slightly higher energy than the trigonal bipyramid, and because this geometry minimizes ligand−core repulsions, it becomes the lowest-energy geometry for $VH_5$ and $V(CH_3)_5$.

**$Cr(CH_3)_6$ and $CrH_6$.** Unlike octahedral $CrF_6$, in which each ligand faces a core basin, the $Cr(CH_3)_6$ molecule has a $C_{3v}$ distorted trigonal-prism framework. The octahedron of core attractors found for $CrF_6$ has eight triangular faces. However, six ligands can only occupy sites opposite to six of these faces, which would give a very unsymmetrical structure with some rather small bond angles. An alternative geometry for an $MX_6$ molecule is a $D_{3h}$ trigonal-prism geometry. This would have six LO core basins with a trigonal-prism geometry rotated by 60° with respect to the trigonal prism of ligands, in which each of the ligands is positioned opposite to an edge of the trigonal prism of core basins. This geometry reduces ligand−core basin repulsions but does not minimize them. The further lowering of the symmetry to $C_{3v}$ presumably occurs because three of the ligands move toward the centers of the adjacent trapezoidal faces of the distorted trigonal prism, thus reducing their interaction with the core, as shown in Figure 3. This distortion is also shown by the C−Cr−C bond angles, which are 90.6° for the upper three carbon atoms and 77.4° for the lower three. This distortion to $C_{3v}$ lowers the energy of the molecule by about 10 kcal·mol$^{-1}$. The actual molecule has a $C_3$ symmetry as a consequence of the different orientations of the methyl groups.

The $CrH_6$ molecule has a $C_{3v}$ distorted trigonal-prism structure (Figure 4, left), which differs considerably from

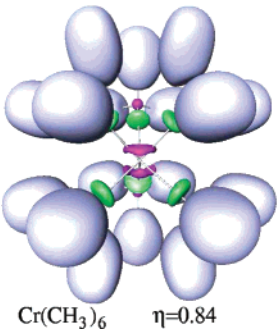


**Figure 3.** ELF localization domains of $Cr(CH_3)_6$. Color code: magenta, cores; green, V(Cr,C); light blue, V(C,H).

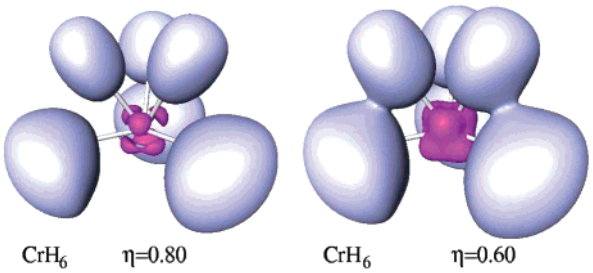


**Figure 4.** ELF localization domains of $CrH_6$ for two values of the isosurface. Color code: magenta, cores; light blue, V(Cr,H).

the structure of $Cr(CH_3)_6$. Three of the H ligands ($H_a$) are in a plane that almost coincides with the Cr atom so that they form H−Cr−H bond angles of 119.6°, while the other three ($H_b$) form H−Cr−H bond angles of 60°. An important feature of this structure is that the distance between each pair of $H_a$ and $H_b$ atoms is only 1.51 Å, which suggests that there is an attractive interaction between them forming weakly bonded $H_2$ molecules bonded to the Cr atom. Figure 4 (right) shows that the V(Cr,$H_a$) and V(Cr,$H_b$) basins tend to merge because the $\eta$ value at the saddle point between them is rather high (i.e., larger than 0.6). The core basin structure is also exceptional in that it is a $C_{3v}$ distorted octahedron, in which only three of the core basins are LO. The three $H_a$ ligands are opposite to three of the faces of the distorted octahedron in positions of minimum interaction with the core, while the other three are in less favorable positions, opposing three of the edges of the distorted octahedron. Presumably, it is the tendency for the formation of $H_2$ molecules that is responsible for the distorted geometry of $CrH_6$.

**$MO_2$ and $MO_3$ Molecules.** All of the $MO_2$ molecules have an angular $C_{2v}$ geometry with bond angles that decrease steadily from $ScO_2^-$ (121.9°) to $CrO_2^{2+}$ (104.3°) and bond lengths that decrease steadily from 163.0 to 150.8 pm (Table 2). All of the $MO_3$ molecules have a triangular-pyramidal $C_{3v}$ geometry with bond angles that decrease from $VO_3^-$ (117.2°) to $MnO_3^+$ (110.6°), and they show a similar decrease in bond lengths from 164.2 to 154.2 pm (Table 2).

The core populations of the $MO_2$ and $MO_3$ molecules are larger than 18, as expected, and are consistently larger than the corresponding $MX_n$ molecules (Table 2). All of the $MO_2$ molecules have four M-shell localization basins with a disphenoidal geometry (Figure 5, left, and Table 5) and the ligands facing two of the faces of the disphenoid of M-shell

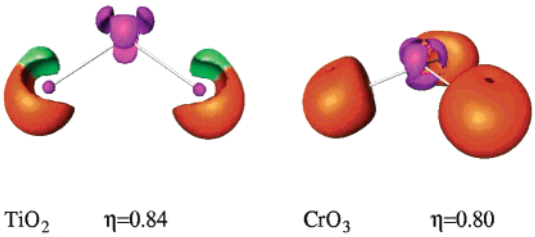


**Figure 5.** ELF localization domains of $TiO_2$ and $CrO_3$. Color code: magenta, cores; green, V(Ti,O); red brick, V(O).

**Table 5.** M-Shell Basins: Number, Type (LO, Ligand Opposed; NLO, Not Opposed; LD, Ligand Directed; CIRC, Toroidal; ax, Axial; eq, Equatorial), ELF Value at the Attractor, Volume ($bohr^3$), and Population

| molecule | group | *n* | type | *η* | *V* | *N* |
|---|---|---|---|---|---|---|
| $ScO_2^-$ | $C_{2v}$ | 4 | 2 LO | 0.889 | 19.71 | 2.08 |
| | | | 2 NLO | 0.877 | 12.29 | 2.36 |
| $TiO_2$ | $C_{2v}$ | 4 | 2 LO | 0.885 | 15.69 | 2.15 |
| | | | 2 NLO | 0.869 | 9.91 | 2.62 |
| $VO_2^+$ | $C_{2v}$ | 4 | 2 LO | 0.872 | 12.71 | 2.28 |
| | | | 2 NLO | 0.855 | 8.56 | 2.82 |
| $Cr_2^{2+}$ | $C_{2v}$ | 4 | 2 LO | 0.850 | 11.55 | 2.63 |
| | | | 2 NLO | 0.829 | 7.05 | 2.88 |
| $VO_3^-$ | $C_{3v}$ | 4 | 3 LO | 0.869 | 7.40 | 2.36 |
| | | | 1 NLO | 0.842 | 7.53 | 3.01 |
| $CrO_3$ | $C_{3v}$ | 4 | 3 LO | 0.860 | 6.96 | 2.45 |
| | | | 1 NLO | 0.815 | 6.08 | 3.53 |
| $MnO_3^+$ | $C_{3v}$ | 4 | 3 LO | 0.844 | 6.39 | 2.47 |
| | | | 1 NLO | 0.818 | 6.67 | 4.47 |

basins, as was observed for the $MX_2$ molecules. All of the $MO_3$ molecules also have four M-shell localization basins with a distorted ($C_{3v}$) tetrahedral geometry (Figure 5, right, $CrO_3$).

The large deviations of the $MO_2$ and $MO_3$ molecules from the linear and planar triangular ($D_{3h}$) VSEPR geometries indicate that there is a strong interaction between the O ligands and the M-shell electrons of the central metal atom. This is consistent with the very short length and presumably great strength of the MO bonds. Overall, it would appear that the strength of the interaction of the ligands with the core increases in the order F < H, $CH_3$ < O.

From the point of view of the ELF topology, these four ligands have different bonding properties. Fluorine forms ionic bonds characterized by the absence of any disynaptic attractor along the bond line. Instead, there is a saddle point on the bond line and the fluorine valence shell attractor is repelled in the direction opposed to the bond. The more covalent M−$CH_3$ bonds are always characterized by a disynaptic V(M,C) basin with a population between 1 and 2. The similar predominately covalent M−H bonds are characterized by protonated disynaptic basins with a population between 1 and 2. The MO bonds in the $MO_3$ molecules are similar to the ionic MF bonds in that there is no disynaptic basin, while in the $MO_2$ molecules, a disynaptic basin is observed, although the attractor is not along the bond line. Conventionally, the MO bonds would be described as polar double bonds $M^{\delta+}{=}O^{\delta-}$. However, no evidence for this description is provided by ELF. It appears that the nature of the MO bond is not yet well understood.

## 5. Summary and Conclusions

1. Deviations of the geometry of the molecules of the period 4 elements in groups 2−12 from the VSEPR geometry are due to the distortion of the M shell by the ligands, each of which produces an opposite-spin pair localization basin, except in the case of $CrH_6$.

2. In $MX_2$ and $MX_3$ molecules, in addition to the two or three LO basins, two additional NLO basins are formed, completing a disphenoidal or trigonal-bipyramidal arrangement of core basins as a consequence of Pauli repulsion between the M-shell electrons.

3. The repulsion between the ligands and the M-shell localization basins can distort the geometry of the molecule from the ligand repulsion or VSEPR geometry. The extent of this distortion depends on the strength of the interaction between the ligands and the M-shell electrons. For the ligands we studied, the strength of this interaction increases in the order F < H, $CH_3$ < O.

4. The strength of the interaction of the F ligand with the core is sufficiently weak such that all of the fluorides we studied, except $CaF_2$, have the ligand repulsion or VSEPR-predicted geometry.

5. The geometry of the molecules with strongly interacting ligands such as H, $CH_3$, and O is determined by the condition that the ligands occupy sites of minimum interaction with the M-shell basins, that is, opposite to the faces of the polyhedron of M-shell basins or in some cases sites of reduced interaction in the edges. This condition leads to the following geometries for the molecules with H, $CH_3$, and O ligands: $MX_2$, angular; $MX_3$, $C_{3v}$ triangular pyramid; $MX_4$, tetrahedral; $MX_5$, $C_{4v}$ square pyramid; $MX_6$, $C_{3v}$ or $C_3$ distorted trigonal prism.

6. The geometry of the molecules we have studied can be summarized as follows:

(a) Weakly interacting ligands, F. The structure predicted by VSEPR or ligand−ligand repulsions: $MX_3$, $D_{3h}$ triangular; $MX_4$, $T_d$ tetrahedral; $MX_5$, $D_{3h}$ trigonal bipyramid; $MX_6$, octahedron. $CaF_2$ is an exception because it is bent not linear as predicted because the distance between the F ligands is large and the F−F repulsion is very weak.

(b) Strongly interacting ligands, H, $CH_3$, and O: $MX_2$, $C_{2v}$ bent; $MX_3$, $C_{3v}$ triangular pyramid; $MX_4$, $T_d$ tetrahedral; $MX_5$, $C_{4v}$ square pyramid; $MX_6$, $C_{3v}$ distorted trigonal prism. $CrH_6$ is very strongly distorted because of H−H interactions.

These results can be regarded as a provisional set of rules for predicting the structure of other $d^0$ molecules of the metals from groups 2−12.

**Acknowledgment.** R.J.G. thanks the Petroleum Research Fund of the American Chemical Society for financial support of this work and Dr. Ian Bytheway and Dr. George Heard for some preliminary calculations.

## Appendix A: Spin Pair Composition

The spin pair composition at a given point of the position space is defined as the ratio of the parallel spin pair concentration by the antiparallel spin pair concentration.[11] It describes the local pairing behavior of the electron cloud in the neighborhood of this point. The information has to be extracted from the spin components of the two-particle density distribution:

$$\pi(\mathbf{r},\mathbf{r}') = \pi^{\alpha\alpha}(\mathbf{r},\mathbf{r}') + \pi^{\alpha\beta}(\mathbf{r},\mathbf{r}') + \pi^{\beta\alpha}(\mathbf{r},\mathbf{r}') + \pi^{\beta\beta}(\mathbf{r},\mathbf{r}') \quad (2)$$

The integrated same-spin pair density within a given finite volume $V(\mathbf{r})$ surrounding the reference point $\mathbf{r}$ is

$$\bar{N}_{||}(\mathbf{r}) = \int_V\int_V \pi^{\alpha\alpha}(\mathbf{r}_1,\mathbf{r}_2)\, d\mathbf{r}_1\, d\mathbf{r}_2 + \int_V\int_V \pi^{\beta\beta}(\mathbf{r}_1,\mathbf{r}_2)\, d\mathbf{r}_1\, d\mathbf{r}_2 \quad (3)$$

whereas the antiparallel pair is

$$\bar{N}_{\perp}(\mathbf{r}) = \int_V\int_V \pi^{\alpha\beta}(\mathbf{r}_1,\mathbf{r}_2)\, d\mathbf{r}_1\, d\mathbf{r}_2 + \int_V\int_V \pi^{\beta\alpha}(\mathbf{r}_1,\mathbf{r}_2)\, d\mathbf{r}_1\, d\mathbf{r}_2 \quad (4)$$

and the sample population $\bar{N}(\mathbf{r})$ is

$$\bar{N}(\mathbf{r}) = \int_V \rho(\mathbf{r}_1)\, d\mathbf{r}_1 \quad (5)$$

The ratio

$$D_{\text{anti}}(\mathbf{r}) = \bar{N}_{||}(\mathbf{r})/\bar{N}_{\perp}(\mathbf{r}) \quad (6)$$

tends to zero in the region of perfect antiparallel pairing and to infinity in those regions dominated by parallel pairs. However, the value of $D_{\text{anti}}(\mathbf{r})$ depends on the size of the sample. This dependence is a simple power law in $\bar{N}(\mathbf{r})^{2/3}$ and, therefore, the size-independent spin pair composition

$$c_\pi(\mathbf{r}) = \bar{N}(\mathbf{r})^{-2/3}\frac{\bar{N}_{||}(\mathbf{r})}{\bar{N}_{\perp}(\mathbf{r})} \quad (7)$$

The localization function $\eta(\mathbf{r})$ is deduced from the spin pair composition by a cosmetic transformation confining its values in the [0, 1] range, i.e.,

$$\eta(\mathbf{r}) = (1 + c_\pi^2(\mathbf{r}))^{-1} \quad (8)$$

It has been shown that the ELF function of Becke and Edgecombe[8] constitutes an excellent approximation to the localization function defined previously. ELF has a rather simple expression in terms of molecular orbitals, which enables one to calculate analytically the derivatives required by the topological partition.

## Appendix B: Basin Populations and Related Quantities

From a quantitative point of view, the integration of the one-electron density over the basin volumes enables one to define the basin populations $\bar{N}(\Omega)$:

$$\bar{N}(\Omega) = \int_\Omega \rho(\mathbf{r})\, d\mathbf{r} \quad (9)$$

as well as their variance $\sigma^2(\Omega)$.[37,38]

$$\sigma^2(\bar{N};\Omega_i) = \sum_{j\neq 1} \bar{N}(\Omega_i)\,\bar{N}(\Omega_j) - \int_{\Omega_i}\int_{\Omega_j} \pi(\mathbf{r}_1,\mathbf{r}_2)\, d\mathbf{r}_1\, d\mathbf{r}_2 = \sum_{j\neq 1} C(\Omega_i,\Omega_j) \quad (10)$$

which is a measure of the quantum mechanical uncertainty of the basin population, which can be interpreted as a consequence of the electron delocalization, whereas the pair covariance $C(\Omega_i,\Omega_j)$ indicates how much the population fluctuations of two given basins are correlated.

IC0354015

(37) Savin, A.; Silvi, B.; Colonna, F. *Can. J. Chem.* **1996**, *74*, 1088.
(38) Noury, S.; Colonna, F.; Savin, A.; Silvi, B. *J. Mol. Struct.* **1998**, *450*, 59.